

1
2
3
4
5
6
7
8
9
10
11
12
13
14
15
16
17
18
19
20
21
22
23
24
25
26
27
28
29
30
31

Bacterial FtsZ induces mitochondrial fission in human cells

Anna Spier^{1,2,3,4,\$}, Martin Sachse⁵, Nam To Tham^{1,2,3,\$}, Mariette Matondo^{6,7}, Pascale Cossart^{1,2,3}, and Fabrizia Stavru^{1,2,3,8,\$,#,*}

¹ Unité des Interactions Bactéries-Cellules, Institut Pasteur, Paris, France

² Institut National de la Santé et de la Recherche Médicale (INSERM), U604, Paris, France

³ Institut National de la Recherche Agronomique (INRA), USC2020, Paris, France

⁴ Université Paris Diderot, Sorbonne Paris Cité, Paris, France

⁵ Unité Technologie et service BioImagerie Ultrastructurale, Institut Pasteur, Paris, France

⁶ Plateforme Protéomique, Unité de Spectrométrie de Masse pour Biologie (UTechS MSBio), Institut Pasteur, Paris, France

⁷ Centre National de la Recherche Scientifique (CNRS), USR 2000, Paris, France

⁸ CNRS SNC5101, Paris, France

^{\$} present address : Unité de Biologie Evolutive de la Cellule Microbienne, Institut Pasteur, Paris, France

[#] CNRS ERL6002, Paris, France

* Correspondence and requests for materials should be addressed to

fabrizia.stavru@pasteur.fr, lead contact

Keywords: mitochondrial division, bacterial division, Drp1, mtDNA, inner mitochondrial membrane

32 **Abstract**

33 Mitochondria are key eukaryotic organelles that evolved from an intracellular bacterium,
34 in a process involving bacterial genome rearrangement and streamlining. As
35 mitochondria cannot form *de novo*, their biogenesis relies on growth and division. In
36 human cells, mitochondrial division plays an important role in processes as diverse as
37 mtDNA distribution, mitochondrial transport and quality control. Consequently, defects
38 in mitochondrial division have been associated with a wide range of human pathologies.
39 While several protists have retained key components of the bacterial division machinery,
40 none have been detected in human mitochondria, where the dynamin-related protein
41 Drp1, a cytosolic GTPase is recruited to the mitochondrial outer membrane, forming
42 helical oligomers that constrict and divide mitochondria. Here, we created a human codon
43 optimized version of FtsZ, the central component of the bacterial division machinery, and
44 fused it to a mitochondrial targeting sequence. Upon expression in human cells, mt-FtsZ
45 was imported into the mitochondrial matrix, specifically localizing at fission sites prior to
46 Drp1 and significantly increasing mitochondrial fission levels. Our data suggests that
47 human mitochondria have an internal, matrix-localized fission machinery, whose
48 structure is sufficiently conserved as to accommodate bacterial FtsZ. We identified
49 interaction partners of mt-FtsZ, and show that expression of PGAM5, FAM210, SFXN3 and
50 MTCH1 induced mitochondrial fission. Our results thus represent an innovative approach
51 for the discovery of novel critical mitochondrial fission components.

52

53

54 **Introduction**

55 Mitochondria are key eukaryotic organelles, which have retained their own genome and
56 are delimited by two membranes. The bacterial origin of mitochondria originally
57 proposed by Lynn Margulis (then Lynn Sagan¹) is now largely accepted, and even complex
58 mitochondrial features, such as the inner mitochondrial membrane invaginations termed
59 cristae, have recently been shown to be evolutionarily conserved in specific bacterial
60 lineages². However, one conundrum is the apparent lack of evolutionary conservation of
61 the division machinery between bacteria and mitochondria of fungi and metazoa.

62 Division is an essential process for both bacteria and mitochondria. In the vast
63 majority of bacteria, cell division is performed by a multiprotein complex, at the heart of
64 which lies the tubulin homologue and evolutionarily conserved protein FtsZ³⁻⁵. In
65 bacteria, FtsZ assembles early at prospective fission sites, forming the Z-ring and
66 recruiting several additional proteins to mediate cell division (reviewed in ^{6,7}).

67 Mitochondrial fission is necessary for proper distribution of the organelle during
68 mitosis and in highly polarized cells⁸ and the dynamic equilibrium between fission and
69 fusion is tightly connected to mitochondrial function in both human and yeast cells⁹. At
70 the molecular level, important differences exist between organisms. While several
71 protists have retained key components of the bacterial division machinery, none have
72 been detected in fungi and metazoa¹⁰, where mitochondrial fission is thought to be
73 governed by a cytosolic machinery¹¹. An intermediate situation has been described in the
74 red alga *Cyanoschizon merolae*, where assembly of an intramitochondrial FtsZ-based
75 fission machinery appears coordinated with the assembly of a cytosolic Dynamin-based
76 fission machinery^{12,13}. In human cells a series of events involving the ER, the actin and
77 septin cytoskeleton and receptors on the mitochondrial outer membrane (OMM)
78 culminates in the assembly of a dynamin-related protein (Drp1) on the OMM⁸; Drp1 then
79 constricts mitochondria, leading to division, with potential synergistic action of Dyn2¹⁴⁻
80 ¹⁶. Fission ensues after constriction beyond a critical threshold¹⁷. During mitochondrial
81 fission the two membranes that delimit mitochondria represent a challenge, as fusion
82 between the outer and inner mitochondrial membranes has to be prevented to avoid
83 leakage of mitochondrial content (Fig 1A). One possible scenario is that the inner
84 membranes reach the necessary curvature and fusogenic distance earlier than the outer
85 membrane, spontaneously fuse and retract, leaving only the outer membranes to fuse,
86 leading to abscission of the two daughter mitochondria. Other scenarios invoke the

87 presence of molecular machineries that either “insulate” the outer from the inner
88 membrane during fission, or that specifically promote fission of the matrix compartment.
89 The latter hypothesis appears the most likely, as a matrix-localized, “bacteria-like” fission
90 machinery with homologs of the bacterial division protein FtsZ at its core has been
91 identified in several protists^{10,18–21}. In light of the monophyletic origin of mitochondria,
92 we and others postulated that metazoan mitochondria would also harbour a fission
93 machinery located in the matrix^{8,22}. Indeed, fission of the matrix compartment has been
94 observed in the absence of outer membrane fission in several metazoans^{23–26}. However,
95 previous attempts at bioinformatic identification of a bacteria-derived division
96 machinery in metazoan mitochondria based on sequence similarity have failed^{10,27}. We
97 hypothesized that the internal fission machinery of mitochondria might nevertheless
98 have retained a certain degree of structural conservation with respect to its bacterial
99 ancestor. To test this hypothesis, we asked whether the key orchestrator of bacterial cell
100 division FtsZ would be able to induce mitochondrial fission in mammalian cells. We
101 engineered synthetic constructs that allowed targeting of bacterial FtsZ into the
102 mitochondrial matrix and found that alphaproteobacterial FtsZ (mt- α FtsZ) specifically
103 localized at mitochondrial fission sites and substantially increased mitochondrial fission
104 levels. As several proteins concur to recruit FtsZ to the membrane in bacteria, we explored
105 which mitochondrial proteins might play this role in our experimental system. Among the
106 interaction partners of mt- α FtsZ that we identified, we tested five transmembrane
107 mitochondrial proteins, four of which induce mitochondrial fission upon overexpression,
108 potentially representing new players in mammalian mitochondrial dynamics.

109

110 **Results**

111

112 **Mitochondrial expression of alphaproteobacterial FtsZ induces mitochondrial** 113 **fission**

114 To achieve fission of the mitochondrial matrix compartment, we hypothesized that
115 mammalian mitochondria would contain a protein-based inner fission machinery (IFM).
116 Given the endosymbiotic origin of mitochondria, we reasoned that the IFM would not
117 have evolved *de novo* and even though not detectable by sequence similarity^{10,27}, it would
118 still share structural features with the bacterial fission machinery.

119 To test whether mitochondria contain an IFM in the matrix that can interact with a
120 bacterial fission protein, we decided to transiently express bacterial FtsZ in human cell
121 lines (U2OS and HeLa). To this end, we constructed synthetic versions of FtsZ, which were
122 codon-optimized for expression in human cells and fused to an N-terminal mitochondrial
123 targeting sequence to allow import into the mitochondrial matrix, and a C-terminal tag to
124 allow detection (Fig 1B). Although mitochondria have long been thought to derive from
125 alphaproteobacteria²⁸⁻³³, recent work suggests that mitochondria evolved from a
126 proteobacterial lineage which branched off before the alphaproteobacteria³⁴. As the
127 precise bacterial lineage that gave rise to mitochondria remains a matter of debate, we
128 chose to express synthetic versions of both gamma- and alphaproteobacterial FtsZ
129 (*Escherichia coli* and typhus group *Rickettsia* respectively, referred to as mt- α FtsZ and mt-
130 γ FtsZ). Immunofluorescence analysis of flag-tagged mt- α FtsZ showed that it localized to
131 mitochondria (Fig 1C) in virtually all transfected cells (99.5 \pm 1.7%, n=1469, N=6
132 independent experiments). In 0.5 \pm 1.6% mt- α FtsZ was expressed at very high levels,
133 formed filaments that colocalized with microtubules (Suppl. Fig 1A) and displayed
134 dramatic mitochondrial fragmentation and perinuclear aggregation (suppl Fig 1B). In
135 cells where mt- α FtsZ localized to mitochondria, those with intermediate and low levels
136 of expression allowed the detection of mt- α FtsZ punctae, which appeared to accumulate
137 at mitochondrial matrix constrictions. In contrast, mt- γ FtsZ or the control construct mt-
138 GFP did not accumulate at constrictions and often displayed a more even staining (Fig 1C).
139 We then tested a C-terminal deletion mutant of mt- α FtsZ (mt- α FtsZ Δ CT) and found that
140 it was able to polymerize in some cells (Fig 1C, suppl Fig 1C), but failed to localize at
141 constrictions, in agreement with previous findings showing that while C-terminal deletion
142 mutants of FtsZ are able to polymerize in *E.coli*, they do not support bacterial division³⁵.

143 Next, we asked whether the ultrastructure of mitochondrial constrictions was
144 affected by mt- α FtsZ. To do so we combined light microscopy with high pressure freezing
145 electron microscopy in a correlative approach allowing us to focus on cells with
146 intermediate expression levels. Mitochondrial constrictions did not qualitatively differ
147 between mt-GFP and mt- α FtsZ expressing mitochondria, which displayed an inner
148 diameter of 41.6nm versus 40.8nm respectively and an outer diameter of 57.1nm versus
149 62.7nm (suppl Fig 1D).

150 Given that mt- α FtsZ was found at constriction sites, we analysed whether it would
151 induce mitochondrial fission by quantifying mitochondrial morphology with the semi-

152 automatic ImageJ plugin MiNA. This analysis showed that full length mt- α FtsZ induced
153 mitochondrial fission (Fig 1C, suppl Fig 1E). We validated our results by using a different
154 cell line (HeLa) and manually measuring mitochondrial length (suppl. Fig 1F), which
155 revealed a dose-dependent effect on mitochondrial fission. In addition, the slightly thicker
156 mitochondria of HeLa cells allowed us to discern mt- α FtsZ -labelled matrix constrictions
157 with non-constricted outer membrane, supporting previous reports showing that matrix
158 constriction can occur in the absence of outer membrane constriction^{25,26}.

159 These data show that in contrast to mt- γ FtsZ, mt- α FtsZ specifically localizes to
160 mitochondrial matrix constrictions and affects mitochondrial morphology, suggesting
161 that it labels mitochondrial matrix fission sites.

162

163 **mt- α FtsZ localizes at mitochondrial fission sites prior to Drp1 recruitment**

164 To assess whether mt- α FtsZ labeled constrictions indeed proceed to complete abscission,
165 we followed GFP tagged mt- α FtsZ in mitochondria of live cells. Full length mt- α FtsZ
166 labeled the vast majority of all fissions we observed (86.3%, n=73, N=6), accumulating at
167 prospective fission sites and often distributing to the tips of both daughter mitochondria
168 upon abscission (Fig 2A). In contrast, the C-terminal deletion mutant mt- α FtsZ Δ CT did
169 not consistently label fission sites (Fig 2B) and was found at up to 1.3 μ m from the fission
170 site in 8 out of 11 fissions (N=4). In agreement with these findings, mt- α FtsZ Δ CT
171 displayed an almost two-fold decrease in inner mitochondrial membrane localization
172 compared to full-length mt- α FtsZ as assessed by immune-electron microscopy (Fig
173 2C/D). In addition, we noticed that mt- α FtsZ induced a zipper-like phenotype with
174 regular, closely apposed cristae, which we also observed by high pressure freezing
175 electron microscopy.

176 Next, we investigated the spatiotemporal relationship between mt- α FtsZ and
177 Drp1. A fraction of endogenous Drp1 colocalized with flag-tagged mt- α FtsZ or
178 accumulated in its close proximity in fixed cells (Fig 2E, yellow and white arrowheads
179 respectively). Live cell imaging revealed that mt- α FtsZ precedes Drp1 recruitment during
180 mitochondrial fission (Fig 2F), suggesting that matrix constriction occurs prior to outer
181 membrane constriction by Drp1. In agreement with this hypothesis, we found matrix
182 constrictions that were labelled with mt- α FtsZ in the absence of outer membrane
183 constriction (suppl Fig 2).

184 Together, these data indicate that matrix-localized mt- α FtsZ is a *bona fide* marker
185 for mitochondrial fission sites and supports a fission model in which matrix constriction
186 precedes Drp1 recruitment and mitochondrial abscission.

187

188 **Replication of the mitochondrial nucleoid is not necessary for mt- α FtsZ localization**

189 The punctate pattern of mt- α FtsZ localization is reminiscent of nucleoids, which have
190 been shown to accumulate at the tips of mitochondria^{36,37}. We therefore assessed the
191 spatial organization of mt- α FtsZ relative to nucleoids and found that mt- α FtsZ was
192 excluded from the area occupied by nucleoids (Fig 3A), in particular at mitochondrial
193 constrictions (suppl Fig 3). However, we also detected instances where mt- α FtsZ partially
194 colocalized with nucleoids (Fig 3A, arrowheads). We hypothesized that this subset could
195 represent replicating nucleoids, which have been estimated to amount to 9% of the total
196 nucleoid population³⁸ and to mark fission sites in yeast and human^{39,40}. We thus examined
197 whether mt- α FtsZ would colocalize with a red version of the mitochondrial DNA
198 polymerase processivity subunit 2 (POLG2-mScarlet), which labels actively replicating
199 mtDNA³⁹. Surprisingly, mt- α FtsZ and POLG2 did not appear to substantially colocalize
200 (Fig 3B).

201 This prompted us to ask whether nucleoid replication was necessary for mt- α FtsZ
202 localization and/or fission. We inhibited mtDNA replication with dideoxycytosine
203 (ddC⁴¹). ddC treatment caused the nucleoid packing protein TFAM-GFP to label the entire
204 matrix compartment, reflecting mtDNA depletion (Fig 3C). In contrast, mt- α FtsZ
205 localization was not affected, marking mitochondrial fission sites in ddC treated and
206 control cells (Fig3C/D). Together, these data strongly suggest that mt- α FtsZ localization
207 is not dependent on nucleoid replication.

208

209 **Identification of mitochondrial proteins that interact with mt- α FtsZ**

210 The dynamic localization of mt- α FtsZ during mitochondrial fission suggests that it
211 interacts with a matrix-localized mitochondrial fission machinery. We therefore sought
212 to identify interaction partners of mt- α FtsZ. To this end, we immunoprecipitated Flag-
213 tagged mt- α FtsZ or mt-GFP from transiently transfected HeLa cells in presence of non-
214 ionic detergent (0.5% NP40), and identified co-precipitating proteins by quantitative
215 mass spectrometry. We identified 941 proteins, which only coprecipitated with mt- α FtsZ,

216 but not with mt-GFP. In addition, 119 proteins were detected in both samples, but were
217 significantly enriched in mt- α FtsZ immunoprecipitates (Fig 4A). 75% of the proteins we
218 identified were not mitochondrial, reflecting mt- α FtsZ interactions taking place prior to
219 its mitochondrial import and cells where mt- α FtsZ mislocalized to the cytoplasm due to
220 high overexpression. As mislocalized mt- α FtsZ colocalizes with microtubules (suppl Fig
221 1A/B), we were not surprised to detect numerous proteins associated with microtubules
222 among our hits. Interestingly, previous experiments have shown that *E.coli* FtsZ
223 expressed in the cytosol of mammalian cells does not spontaneously colocalize with
224 tubulin⁴², suggesting important structural differences between alpha- and
225 gammaproteobacterial FtsZ. Among the overall 1060 interactants of mt- α FtsZ, 31.7%
226 were organellar proteins and 25% (i.e. 269) mitochondrial according to the mitochondrial
227 protein database IMPI (Integrated Mitochondrial Protein Index, v2018_Q2), despite the
228 fact that we did not purify mitochondria prior to immunoprecipitation, reflecting an ~3
229 fold enrichment in mitochondrial proteins if compared with ~8% mitochondrial proteins
230 in the human genome^{43,44}. Consistently, Gene Ontology term analysis showed significant
231 enrichment of organellar proteins, and in particular mitochondrial proteins (Fig 4B and
232 suppl fig 4). Our dataset contained several inner and outer mitochondrial membrane
233 proteins that have been linked to mitochondrial morphology or division (e.g. MICOS
234 complex proteins Mic60, Mic27 and Mic19^{45,46}, Prohibitin 2 and SPY complex members
235 Yme1L and Stomatin-like protein 2⁴⁷, mitochondrial fission protein 1 (Fis1⁴⁸),
236 mitochondrial fission process protein 1 (MTFP1/MTP18⁴⁹), ATAD3B⁵⁰, SLC25A46A¹ and
237 AFG3L2⁵¹, reinforcing our hypothesis that mt- α FtsZ can interact with an endogenous
238 mitochondrial matrix fission machinery. Gene ontology analysis with the DAVID software
239 highlighted an enrichment in mitochondrial inner membrane proteins (suppl fig 4A).
240 Indeed, 74 of the 269 mitochondrial proteins (27.5%) we identified were predicted to
241 contain at least one transmembrane domain. Interestingly, previous *in vitro*
242 reconstitution experiments have shown that FtsZ cannot mediate unilamellar liposome
243 constriction without its membrane-anchoring partner FtsA⁵². We therefore chose to focus
244 on five highly enriched transmembrane proteins, the mitochondrial serine-threonine
245 phosphatase PGAM5, MTCH1 (mitochondrial carrier homolog 1), FAM210A, the ATP
246 synthase membrane subunit DAPIT (diabetes-associated protein in insulin-sensitive
247 tissue) and SFXN3 (Sideroflexin 3). We selected these proteins based on their enrichment
248 score and their detection in independent immunoprecipitation experiments, where beads

249 were used as a control (not shown). Among the selected candidates, MTCH1, DAPIT and
250 FAM210A have not been studied in the context of mitochondrial dynamics, while recent
251 data has implicated PGAM5 in mitochondrial dynamics⁵³⁻⁵⁵ and in the course of this study
252 members of the Sideroflexin family have been shown to act as serine transporters and
253 impact mitochondrial morphology⁵⁶.

254 We employed Flag-tagged versions to confirm mitochondrial localization of the
255 five selected candidates and assess their impact on mitochondrial morphology.
256 Morphometric analysis (MiNa) revealed that PGAM5, MTCH1, FAM210A and SFXN3
257 induced significant mitochondrial fission (Fig 4C, suppl Fig 4B). This phenotype was not
258 a by-product of non-specific inner membrane perturbation due to overexpression, as even
259 strong overexpression of DAPIT had no detectable effect on mitochondrial morphology.
260 At very low expression levels, flag-tagged PGAM5, MTCH1, FAM210A and SFXN3 were
261 also found at mitochondrial matrix constrictions (Fig 4D), supporting a possible role in
262 matrix fission. Attempts to follow the sub-mitochondrial localization of these candidates
263 in live cells using GFP fusions failed because their overexpression induced mitochondrial
264 fission or substantially mislocalized to the cytoplasm (not shown). Silencing of the
265 individual proteins did not robustly induce mitochondrial hyperfusion, and did not
266 prevent localization of mt- α FtsZ to mitochondrial constrictions (not shown), suggesting
267 possible functional redundancy. Co-silencing of two or more proteins resulted in high
268 toxicity (not shown).

269 In conclusion, we propose that PGAM5, MTCH1, FAM210A and SFXN3 represent
270 novel candidate effectors of inner mitochondrial membrane fission.

271 Discussion

272 Fission of the mitochondrial matrix in the absence of outer membrane fission has been
273 shown in metazoans, both *in vivo*²⁴ and *in cellulo*^{23,25,26}. How this is achieved is unclear.
274 Although in several protozoa orthologs of the key bacterial fission protein FtsZ have been
275 shown to localize to the mitochondrial matrix and participate to mitochondrial
276 division^{12,19,20}, FtsZ orthologs have not been detected in metazoans and fungi^{10,27}. Here,
277 we show that when directed into human mitochondria, alphaproteobacterial FtsZ (mt-
278 α FtsZ) localizes at mitochondrial fission sites and stimulates mitochondrial division.
279 Interestingly, expression of mitochondrial FtsZ from the brown alga *Mallomonas*
280 *splendens* in yeast was found to affect mitochondrial morphology¹⁹. Together, this data

281 suggest that human and yeast mitochondria contain a matrix-localized fission machinery
282 that is structurally similar to the bacterial division machinery, as it can accommodate
283 heterologously expressed FtsZ, indicating that mt- α FtsZ has retained features that allow
284 it to interact productively with the inner fission machinery of today's mitochondria.

285 Surprisingly, when we compared FtsZ from an alphaproteobacterium (mt- α FtsZ)
286 with that from a gammaproteobacterium (mt- γ FtsZ), only mt- α FtsZ formed stable
287 assemblies that localize at mitochondrial fission sites. Polymerization is not unexpected
288 *per se*, as purified FtsZ has been shown to spontaneously assemble into polymers upon
289 GTP addition⁵⁷. One possibility is that mt- γ FtsZ polymers are unstable, as they are unable
290 to interact with the mitochondrial matrix fission machinery, which manifests by lack of
291 localization to mitochondrial constrictions. Another possibility is that, coming from *E.coli*,
292 mt- γ FtsZ has adapted to the diameter of the bacterium, ($\sim 0.5\mu\text{m}$ ⁵⁸) and therefore cannot
293 form rings in mitochondria due to spatial constraints imposed by the narrower diameter
294 of mitochondria ($\sim 0.2\mu\text{m}$ ⁵⁹). In contrast mt- α FtsZ may have an inherent ability to adapt
295 to smaller diameters, as Rickettsiae have diameters as small as $0,1\mu\text{m}$ ⁶⁰.

296

297 **How are the sites of mt- α FtsZ assembly determined?**

298 The question of how the division site is defined is central also in bacterial division. In *E.*
299 *coli*, the best-studied model, two negative regulatory mechanisms have been described,
300 based on nucleoid occlusion or on the Min system⁶¹. No orthologs for either of these
301 systems have been detected in mitochondria¹⁰, where the nucleoid has been suggested to
302 act as a spatial organizer of the mitochondrial fission machinery. Consistent with this
303 view, mitochondrial fission and mtDNA dynamics are tightly linked in the red alga
304 *Cyanidioschizon merolae*⁶². In mammalian cells, up to 70% of all fission events have been
305 found to occur in the vicinity of a nucleoid⁴¹ and components of the outer (cytosolic)
306 fission machinery have been suggested to sense the localization and replication status of
307 nucleoids³⁹. In our hands the localization of mt- α FtsZ and mitochondrial morphology
308 were not affected by blocking mtDNA replication (Fig 3C), suggesting that this process is
309 not essential for IFM assembly and localization. Interestingly, in nucleoid-free *E. coli*
310 maxicells FtsZ localized to the midcell in a Min system - dependent manner⁶³. As the Min
311 system is not conserved in human mitochondria¹⁰, how mt- α FtsZ localizes to fission sites
312 in the absence of nucleoids remains an open question. One possibility is that it is the inner
313 mitochondrial fission machinery and its associated proteins, such as the constituents of

314 contact sites or possibly lipid microdomains, that define mtDNA localization; this
315 situation is similar to what has been observed for the mtDNA helicase Twinkle, which can
316 associate with the inner mitochondrial membrane in the absence of mtDNA³⁸.

317

318 **How does mt- α FtsZ induce mitochondrial fission at the mechanistic level?**

319 mt- α FtsZ clearly labels mitochondrial fission sites and stimulates fission, but we currently
320 do not know how it functions and whether it displaces components of the endogenous
321 IFM or not. In bacteria, FtsZ has been proposed to mediate constriction either
322 directly^{57,64,65}, or indirectly, i.e. by recruiting the peptidoglycan synthesis machinery⁶⁶⁻⁶⁸.
323 Mitochondria have lost the peptidoglycan, but mt- α FtsZ might act by recruiting the lipid
324 biosynthesis machinery. In agreement with this hypothesis, we found several proteins
325 involved in lipid synthesis among the interactors of mt- α FtsZ. However, we cannot
326 exclude that mt- α FtsZ acts in a more direct manner, i.e. by physically pulling on the inner
327 membrane to promote fission of the matrix compartment. The interactions that allow the
328 recruitment of FtsZ to its membrane anchors FtsA, ZipA or SepF are mediated by the C-
329 terminus of the protein, which is essential for promoting fission⁷. In agreement with this,
330 the C-terminus of mt- α FtsZ was essential to localize the protein to the mitochondrial
331 inner membrane and its deletion abolished mitochondrial fission induction. *In vitro*
332 experiments have shown that while FtsZ can self-assemble into contractile rings in the
333 absence of other proteins⁶⁵, its recruitment to the membrane requires additional
334 proteins⁵². We employed an immunoprecipitation approach to identify mitochondrial
335 inner membrane proteins that could mediate the recruitment of mt- α FtsZ to the inner
336 mitochondrial membrane. With this approach, we could identify proteins that have been
337 previously implicated in mitochondrial fission and novel potential actors.

338 Here, we focused on five inner membrane proteins with an unclear role in
339 mitochondrial matrix fission: PGAM5, MTCH1, SFXN3, FAM210 and DAPIT.
340 Overexpression of DAPIT did not affect mitochondrial morphology, indicating that
341 overexpression does not *per se* alter mitochondrial morphology, even though the
342 mitochondrial inner membrane is one of the most protein-rich membranes⁶⁹. In contrast,
343 mild overexpression of PGAM5, MTCH1, SFXN3 and FAM210 induced mitochondrial
344 fission. MTCH1 and FAM210 were not previously known to affect mitochondrial
345 dynamics. In our hands, even mild SFXN3 overexpression induced mitochondrial fission,
346 but previous data indicates that double deletion of SFXN3 and SFXN1 in Jurkat cells

347 caused a decrease mitochondrial length⁵⁶. While further studies are needed to untangle
348 the precise role of SFXN3 in mitochondrial dynamics, our data confirms a role of PGAM5
349 in mitochondrial fission and adds FAM210 and MTCH1 to the growing list of inner
350 membrane proteins playing a role in mitochondrial fission.

351 It is intriguing to note that among the interactors of mt- α FtsZ we also found several
352 proteins that have been proposed to link the inner and outer membranes. One is ATAD3B,
353 a paralog of ATAD3A, an AAA+ ATPase shown to control mitochondrial dynamics and to
354 interact with both the inner and outer mitochondrial membranes⁷⁰. We also found the
355 MICOS complex component Mic60, which has been shown to bind to the nucleoid⁷¹ and
356 link it with two outer membrane components (the SAM complex and Metaxins 1 and 2)
357 and with the cytosolic fission machinery^{45,46}. Strikingly, we detected SAMM50 and
358 Metaxin 2 in mt- α FtsZ immunoprecipitates, suggesting at least partial integrity of the
359 complex and providing a mechanism for the observed spatiotemporal coordination of mt-
360 α FtsZ and Drp1 recruitment.

361

362 **Is mt- α FtsZ regulated?**

363 Our live cell imaging experiments showed mt- α FtsZ localization at fission sites prior to
364 Drp1. While we detected mt- α FtsZ at virtually all fission events, not all mt- α FtsZ
365 assemblies underwent fission in a given time frame. This suggests that either only a subset
366 of mt- α FtsZ oligomers are functional, or that the IFM is preassembled and poised to act
367 upon specific triggering signals, similar to the cytosolic fission machinery based on
368 Drp1⁷². A triggering signal for the IFM may be local calcium influx at ER-mitochondrial
369 contact sites. Indeed, calcium influx has been shown to induce mitochondrial matrix
370 fission, followed by outer membrane abscission²⁶. Consistent with a role of calcium in the
371 regulation of mitochondrial matrix fission, we found several regulators of mitochondrial
372 calcium influx among the proteins that co-immunoprecipitated with mt- α FtsZ.
373 Incidentally, divalent cations (including calcium) also stimulate FtsZ assembly and
374 bundling in bacteria, pointing to an evolutionarily conserved regulatory mechanism of
375 division^{7,73}.

376

377 In conclusion, our work suggests the presence of a mitochondrial fission machinery in the
378 mitochondrial matrix that retained sufficient structural conservation to accommodate a
379 heterologously expressed bacterial FtsZ. To our knowledge, this represents the first *bona*

380 *fide* marker of matrix fission sites described to date and paves the way for the molecular
381 characterization of the mitochondrial matrix fission machinery. Future experiments will
382 address whether FtsZ from other bacterial species have retained the ability to
383 consistently label mitochondrial fission sites and interact with the inner mitochondrial
384 fission machinery. Our system may thus also provide a novel “evolutionary cell biology”
385 approach to understand which bacteria represent the closest extant relatives of
386 mitochondria and shed light on the debated origin of the bacterial ancestor of
387 mitochondria.

388

389 **Material and Methods**

390 **Cloning**

391 To create humanized versions of gammaproteobacterial FtsZ, the *E.coli* FtsZ sequence was
392 completely re-coded according to human codon usage to optimize expression in human
393 cells. To comply with local regulations, for alphaproteobacterial FtsZ, we used the *R.typhii*
394 sequence as to re-code the N-terminal part (aa 2-326) of FtsZ, and the *R.prowazekii*
395 sequence to re-code the C-terminal domain. For both constructs, we deleted the initial
396 methionine to prevent internal initiation and the terminal stop codon was replaced with
397 a glycine-serine linker to allow in-frame expression of a Flag or a GFP tag. Re-coded
398 sequences were synthesized by Genecust or as gBlocks (Integrated DNA Technologies).
399 OM-mRuby was generated by in-frame fusion of the first 215bp of human TOM20 (gBlock,
400 Integrated DNA Technologies) with mRuby. All constructs are listed in table M1.

401

402 **Reagents**

403 Chemicals: Orange and Deep Red Mitotracker and secondary antibodies were purchased
404 from Thermo Fisher. All chemicals were obtained from Sigma-Aldrich/Merck. Complete
405 mini EDTA-free protease inhibitor and PhoStop phosphatase inhibitor tablets were from
406 Roche, anti-Flag M2 dynabeads were from Sigma-Aldrich/Merck.

407 Antibodies: Antibody sources are detailed in table M2. All antibodies were used according
408 to the manufacturer’s instructions unless otherwise stated.

409

410 **Cell culture and transfection**

411 HeLa and U2OS cells were obtained from ATCC and cultured under standard conditions;
412 media and additives were from Thermo Fisher. Cells were seeded on coverslips (#1.5,
413 Marienfeld) for immunofluorescence or MatTek dishes (MatTek Corporation) for live cell
414 imaging and transfected with FugeneHD (Roche) according to the manufacturer’s
415 instructions, at a DNA:transfectant rate of 1:3. The DNA quantities employed for each
416 construct are indicated in table M1. Cells were imaged or fixed and processed for
417 immunofluorescence 24h-36h posttransfection.

418

419 **Immunofluorescence and imaging**

420 Cells grown on coverslips were stained with mitotracker when necessary, fixed for 10
421 minutes in 4% paraformaldehyde (Electron Microscopy Sciences)/PBS, washed in PBS
422 and permeabilized for 5 minutes in 0.1% Triton X-100 in PBS and blocked for at least 30

423 minutes in 1% BSA and 10% goat serum. Primary antibodies (see table M2) were
424 incubated for 60 minutes in blocking buffer, followed by three washes in PBS (5 minutes)
425 and incubation with Hoechst 33258 and Alexa-labelled secondary antibodies (Thermo
426 Fisher) in blocking buffer for 30 minutes. Coverslips were then washed extensively in PBS
427 and mounted in Vectashield (Vector Laboratories). For live cell imaging, cells grown on
428 Mattek dishes were stained with mitotracker when necessary, then imaged in Fluorobrite
429 medium (Thermo Fisher) on a Roper spinning disk confocal system (Zeiss
430 AxioObserver.Z1 inverted fluorescence microscope equipped with an Evolve EM-CCD
431 camera (Photometrics) and a Yokogawa CSU-X1 spinning disc). Images were acquired at
432 37°C with a 100x NA 1.4 oil objective using MetaMorph. Cells were imaged every 20
433 seconds for 10 or 15 minutes.

434

435 **Image analysis**

436 All images were analyzed in ImageJ/Fiji (National Institutes of Health), including
437 adjustment of brightness and contrast. Overlays were assembled in Photoshop (Adobe)
438 and figure panels in Illustrator (Adobe). The ImageJ macro Mitochondrial Network
439 Analysis (MiNA) toolset⁷⁴ was used to examine mitochondrial morphology. Single cells
440 were selected as regions of interest and pre-processing parameters were adjusted in
441 order to obtain optimal skeletonized images of the mitochondrial network, followed by
442 extraction of mitochondrial network features such as number of individuals, branch
443 length and mitochondrial area, referred to as “mitochondrial area”. To obtain a degree of
444 mitochondrial fragmentation that would be independent of the size of the mitochondrial
445 network we used the ratio of individual mitochondria and total mitochondrial area.

446

447 **Statistical analysis**

448 Results are expressed as means of at least three independent experiments, error bars
449 represent the standard error of the mean. For multiple comparisons, data were analyzed
450 with the Prism software (Graphpad) by one-way ANOVA, followed by Dunnett’s multiple
451 comparisons test to obtain the adjusted P value. Significance is indicated as $p < 0.05$ (*),
452 $p < 0.01$ (**), $p < 0.005$ (***), ns for $p > 0.05$. N refers to the number of independent
453 experiments, n refers to the number of counted events (cells, individual mitochondria,
454 fissions).

455

456 **Electron microscopy**

457 Correlative light electron microscopy (CLEM)

458 To obtain landmarks for CLEM the pattern of an HF-15 finder grid (AGAR) was evaporated
459 with carbon on sapphire (3 mm diameter, 0.16 mm thickness, Wohlwendt instruments)
460 as described⁷⁵. The discs with stabilized carbon pattern were sterilized by UV and coated
461 with poly-L-Lysine (Sigma-Aldrich) for cell culture. After transfection, cells were imaged
462 in medium containing 1mM Hepes after placing the disc in a glass bottom dish (MatTek)
463 using a Leica SP5 confocal microscope (Leica) and low expressing cells were selected.
464 After imaging the cells were frozen with an HPM 010 (Abra fluid). Samples were freeze
465 substituted in a Leica AFS2 (Leica microsystems) in 1% osmiumtetroxide, 0.1%
466 uranylacetate, 5% water, 2% MeOH in dry acetone with the following schedule: 1h at -
467 90°C, 2.5°C/h for 16h, 30 min at -50°C, 15°C/h for 2h, 30 min at -20°C, 10°C/h for 2h, and
468 1h at 0°C. After substitution the dishes were infiltrated with epoxy resin (Agar) and
469 polymerization was done in flat bottom beam capsules at 60°C for 48h. After detachment
470 of the discs the sample was sectioned with a Leica UCT microtome (Leica microsystems)
471 with a nominal feed of 70 nm. Sections were picked up with slot grids and contrasted with

472 4% aqueous uranylacetate (Merck) and Leynolds lead citrate (Delta microscopies).
473 Images were taken with a Tecnai G2 microscope operated at 120 kV (Thermofisher),
474 equipped with an ultrascan 4000 CCD (Gatan Inc.).

475 Immuno electron microscopy

476 For immune-labeling on thawed cryo sections cells were fixed with 2% PFA (EMS) + 0.1%
477 glutaraldehyde (Sigma) in PHEM buffer, pH 7 (60 mM Pipes, 25 mM Hepes, 10 mM EGTA,
478 2 mM MgCl₂) for 1 h at RT. Afterwards free aldehyde groups were quenched with 50 mM
479 NH₄Cl in PBS and cells were removed from the culture plastic with a rubber policeman
480 and pelleted in a 1.5 ml eppendorf tube. The cell pellet was embedded in 12% gelatin
481 (TAAB) and after solidification on ice, small cubes of 1 mm³ were cut and infiltrated
482 overnight at 4°C with 2.3 M sucrose in PBS. The next day the cubes were mounted on
483 metal pins and frozen by immersion into liquid nitrogen. Thin sections of 60 nm nominal
484 feed were cut with a Leica UC6/FC6 cryo-microtome at -120°C. The sections were picked
485 up with a 1:1 mixture of 2% methylcellulose in water and 2.3M sucrose in PBS. After
486 thawing the sections were deposited on grids and labelled with rabbit anti GFP
487 (Rockland) followed by Protein A gold (CMC Utrecht). At the end of the labelling the
488 sections were contrasted with 0.4% uranylacetate in 1.8% methylcellulose and airdried
489 before observation with Tecnai G2 microscope. For the quantification of matrix/inner
490 membrane localization of mt- α FtsZ-GFP or its Δ CT version, 36 and 25 random sections
491 were quantified respectively.

492

493 **Immunoprecipitation**

494 Immunoprecipitation was performed as described⁷⁶ with modifications. Briefly, HeLa
495 cells were seeded on 10 cm dishes and transfected with 7 μ g DNA. After 36h, cells were
496 washed three times in PBS and lysed for 30 min with 1 ml lysis buffer/10cm dish (20 mM
497 Tris, pH 7.4, 100 mM NaCl, 10% glycerol, 1,5mM MgOAc) supplemented with 0.5% NP-40
498 (Igepal), 1x protease and phosphatase inhibitors (Roche). Lysis and all subsequent steps
499 were performed at 4 °C. After lysate clarification at 13000xg for 10 minutes, the protein
500 concentration of the supernatant was determined by Bradford assay (Pierce). 1 mg of
501 lysate was incubated overnight with 20 μ l anti-Flag M2 magnetic Dynabeads (Sigma-
502 Aldrich/Merck) under shaking. Magnetic beads were recovered, washed three times with
503 lysis buffer and four times with washing buffer (50 mM Tris, pH 7.4, 150 mM NaCl) and
504 eluted with 2x20 μ l 3xFlag peptide (100 mg/mL in washing buffer). The experiment was
505 performed in triplicate. For western blot, 5 μ l (10%) eluate was supplemented with 2x
506 Laemmli buffer, boiled for 10min resolved on a gradient SDS-PAGE (Biorad), and
507 subjected to western blotting via wet transfer to 0.45 μ m nitrocellulose membrane
508 (Millipore). Ten μ g total lysate were loaded (corresponding to 1%) for the input.

509

510 **Proteomic analysis**

511 Protein digestion: Proteins were solubilized in urea 8 M, NH₄HCO₃ 50 mM pH 7.5, then
512 disulfide bonds were reduced with 5 mM tris (2-carboxyethyl) phosphine (TCEP) for 30
513 min at 23°C and alkylated with 20 mM iodoacetamide for 30 min at room temperature in
514 the dark. Samples were diluted to 1 M urea with 50 mM NH₄HCO₃ pH 7.5, and Sequencing
515 Grade Modified Trypsin (Promega, Madison, WI, USA) was added to the sample at a ratio
516 of 50:1(w/w) of protein to enzyme for 8 h at 37°C. Proteolysis was stopped by adding 1%
517 formic acid. Resulting peptides were desalted using Sep-Pak SPE cartridge (Waters)
518 according to manufactures instructions. Peptides elution was done using a 50%
519 acetonitrile (ACN), 0.1% FA buffer. Eluted peptides were lyophilized and then store until
520 use.

521 **LC-MS/MS analysis:** a nanochromatographic system (Proxeon EASY - nLC 1000, Thermo
 522 Fisher Scientific) was coupled online to a Q Exactive™ Plus Mass Spectrometer (Thermo
 523 Fisher Scientific). For each sample, 1µg of peptides was injected onto a 50 - cm
 524 homemade C18 column (1.9µm particles, 100 Å pore size, ReproSil - Pur Basic C18, Dr.
 525 Maisch GmbH) and separated with a multi - step gradient from 2% to 45% ACN at a flow
 526 rate of 250 nl/min over 180 min. The column temperature was set to 60°C. The data were
 527 acquired as previously described⁷⁷.

528 **Data processing:** Raw data were analyzed using MaxQuant software version 1.5.3.8⁷⁸ with
 529 database search parameters as described in⁷⁷. The MS/MS spectra were searched against
 530 Uniprot proteome database of *Human (January 13, 2015, 20,432 entries)* and mt-αFtsZ-
 531 Flag protein, and usual MS contaminants. Data were quantified with the MaxLFQ
 532 algorithm by requiring a minimum peptide ratio count of 2. The parameter “match
 533 between run” was checked. Raw data have been deposited to the ProteomeXchange
 534 Consortium via the PRIDE⁷⁹ repository with the dataset identifier PXD016722.

535 **Statistical and functional analysis:** For the statistical analysis of one condition versus
 536 another, proteins exhibiting fewer than 2 intensities in at least one condition were first
 537 discarded. After log₂ transformation, intensities were normalized by median centering
 538 within conditions (*normalized* function of the R package DAPAR⁸⁰). Proteins without any
 539 intensity in one condition (quantitatively present in a condition, absent in another) were
 540 considered as differentially abundant. Next, missing values were imputed using the
 541 *imp.norm* function of the R package *norm*. Proteins with a log₂(fold-change) inferior to 1
 542 have been considered as proteins with no significant difference in abundance. Statistical
 543 testing of the remaining proteins was conducted using a limma t-test⁸¹. An adaptive
 544 Benjamini-Hochberg procedure was applied on the resulting p-values to select a set of
 545 significantly differentially abundant proteins with a false discovery rate of 1%⁸². The
 546 proteins of interest are therefore the proteins that emerge from this statistical test
 547 supplemented by those being quantitatively absent from one condition and present in
 548 another. Gene ontology analysis of mass spectrometry results was performed with the
 549 online softwares Panther (<http://pantherdb.org/>) and DAVID
 550 (<https://david.ncifcrf.gov/>), using standard settings. Transmembrane proteins were
 551 predicted using the online software TMHMM
 552 (<http://www.cbs.dtu.dk/services/TMHMM/>).

553 554 **Data availability**

555 The data that support the findings of this study are available from the corresponding
 556 author on reasonable request.

557

558 **Table M1: Plasmids**

559

Expressed protein	Vector backbone	Transfection (µg /Mattek)	reference
mt-αFtsZ-Flag	pEF_cFlag	0.5µg	This study
mt-αFtsZΔCT-Flag	pEF_cFlag	0.5µg	This study
mt-γFtsZ-Flag	pEF_cFlag	0.5µg	This study
mt-GFP-Flag	pEF_cFlag	0.5µg	This study
mt-αFtsZ-GFP	pEF_cGFP	0.5µg	This study
mt-αFtsZΔCT-GFP	pEF_cGFP	0.5µg	This study
PolG-mScarlet	pcDNA3.1	0.5µg	This study
OM-ruby	mRubyC1	0.5µg	This study
TFAM-GFP	pEF_cGFP	0.5µg	This study

PGAM5-myc-Flag	pCMV6_Entry	0.25 µg	Origene
MTCH1-myc-Flag	pCMV6_Entry	0.25 µg	Origene
FAM210A-myc-Flag	pCMV6_Entry	0.25 µg	Origene
SFXN3-myc-Flag	pCMV6_Entry	0.25 µg	Origene
DAPI1-myc-Flag	pCMV6_Entry	0.25 µg	Origene
pDsRed2-mito		0.25 µg	Clontech
Drp1-mCherry		0.5 µg	83

560

561 **Table M2: Antibodies**

562

Antibody	Catalog number	Provider
Tom20	Clone 29	BD Biosciences
Drp1	611112	BD Biosciences
tubulin	Clone B5.1.2	Sigma-Aldrich/Merck
mtDNA	Ac-30-10	Progen
Hsp60	D6F1	Cell Signaling
anti-FLAG	Clone M2	Sigma-Aldrich/Merck

563

564 **Author contributions**

565 AS: Data curation, Formal analysis, Investigation, Methodology; MS: Investigation,
566 Methodology, Writing – review & editing; TNT: Investigation, Methodology; MM:
567 Methodology; FS and PC: Funding acquisition, Writing – review & editing; FS:
568 Conceptualization, Data curation, Formal analysis, Investigation, Methodology,
569 Validation, Visualization, Writing – original draft, Supervision.

570

571 **Acknowledgements**

572 We would like to thank Véronique Hourdel and Quentin Gai Gianetto for initial analysis
573 of mass spectrometry data and Ludmila Bonnand for help with live cell imaging analysis.
574 Alessandro Pagliuso, Jan Riemer and Tim Wai are thanked for discussion and Simonetta
575 Gribaldo, Bastian Huelsmann, Nika Pende, and Hans Spelbrink for critical reading of the
576 manuscript. This study was supported by the European Research Council (H2020-ERC-
577 2014-ADG 670823-BacCellEpi to P.C.) and Institut Pasteur. A.S. was supported by a
578 BioSPC doctoral fellowship from the Université Paris Diderot. P.C. is a Senior International
579 Research Scholar of the Howard Hughes Medical Institute. F.S. is a CNRS permanent
580 researcher.

581

582 **Conflict of Interest**

583 The authors declare no conflict of interest.

584

585 **Figure legends**

586

587 **Fig1: Expression of alphaproteobacterial FtsZ (mt- α FtsZ) in human mitochondria**
588 **induces mitochondrial fission.**

589 **A**

590 Schematic representation of mitochondrial constriction (cross-section), where Drp1 is
591 depicted in turquoise, the outer membrane in blue, the inner membrane in black and the
592 matrix in burgundy. The top arrow points at a theoretical scenario, where fission entails
593 inner and outer membrane fusion. The bottom arrow points at the current fission model,
594 where inner membrane undergoes homotypic fusion, leading to matrix fission. This is
595 then followed by homotypic fusion of the outer membrane to achieve complete abscission
596 of the two daughter mitochondria. *In vivo*, matrix and outer membrane fission appear
597 closely linked in time and space.

598 **B**

599 General layout of the synthetic FtsZ constructs used in this study: a well-characterized
600 mitochondrial targeting sequence (MTS) from subunit 9 of the Fo-ATPase of *N. crassa* was
601 fused at the N-terminus of bacterial FtsZ, which was codon-optimized for expression in
602 human cells. A C-terminal Flag or GFP tag was added for detection. Numbers refer to the
603 alphaproteobacterial construct mt- α FtsZ. A control construct was created by replacing
604 the FtsZ sequence with GFP, resulting in mito-GFP-Flag.

605 **C**

606 Immunofluorescence of U2OS cells transfected with mito-GFP-Flag or mitochondrially
607 targeted FtsZ from a gamma- (mt- γ FtsZ-Flag) or an alphaproteobacterium (mt- α FtsZ-
608 Flag, C-terminal deletion mutant mt- α FtsZ Δ CT-Flag, revealed in green) and mitochondria
609 (Hsp60, red). Scalebar: 10 μ m, insets are enlarged 4-fold. Linescan positions are indicated
610 by a yellow line.

611 **D**

612 Semiautomated quantification (MiNA plugin) of mitochondrial morphology expressed
613 by the amount of individual mitochondria/mitochondrial area in cells transfected as in
614 B. Three experiments were pooled. Mean and SEM are displayed in red, P=0.0002 by
615 one-way Anova, adjusted P-value = 0.0049.

616

617

618 **Fig 2: mt- α FtsZ labels mitochondrial fission sites and precedes Drp1 recruitment**

619 **A**

620 Live cell imaging of U2OS cells transfected with mt- α FtsZ-GFP or mt- α FtsZ Δ CT-GFP.

621 Insets show an example of mitochondrial fission and are enlarged 2x. Linescans were

622 taken for each timepoint along the fission axis. Scalebar: 10 μ m.

623 **B**

624 Post-embedding immuno-EM of HeLa cells transfected with the above constructs,

625 stained with nanogold-anti-GFP. Scalebar: 100 nm.

626 **C**

627 Quantification of nanogold signal with respect to the inner mitochondrial membrane or

628 the matrix (i.e. >15 nm distance from the inner membrane). n indicates the number of

629 analyzed nanogold grains from 36 (mt- α FtsZ-GFP) or 25 random sections (mt-

630 α FtsZ Δ CT-GFP).

631 **D**

632 Colocalization of mt- α FtsZ-GFP (green) with Drp1 (red) in HeLa cells. Mitochondria were

633 stained with mitotracker deep red (blue). Yellow arrowheads point at colocalization

634 between mt- α FtsZ-GFP and Drp1, white arrowheads point at apposition. Inset enlarged

635 2x.

636 **E**

637 Live cell imaging of U2OS cells co-transfected with mt- α FtsZ-GFP and Drp1-mCherry,

638 stained with mitotracker deep red. Insets show an example of mitochondrial fission and

639 are enlarged 2x. mt- α FtsZ-GFP (white arrowhead) is present prior to Drp1 (yellow

640 arrowhead).

641

642 **Fig 3: mt- α FtsZ localizes in proximity of the nucleoid, but is independent of mtDNA**
643 **replication**

644 **A**

645 U2OS cells transfected with mt- α FtsZ-GFP (green) and labeled for mtDNA (red) and

646 mitotracker deep red (blue). Inset enlarged 2x. Linescan showing juxtaposition of green

647 and red signal; arrowheads point at colocalization between mt- α FtsZ and mtDNA.

648 Scalebar: 10 μ m.

649

650 **B**

651 Fluorescence images of U2OS cells transfected with mt- α FtsZ-GFP (green) and POLG-
652 mScarlet (red). Mitochondria are shown in blue (mitotracker deep red). Inset enlarged
653 2x. Linescan showing alternating green and red signal. Scalebar: 10 μ m.

654 **C**

655 U2OS cells treated with 10 μ M ddC or vehicle for 48h, then transfected with mtDsRed
656 and mt- α FtsZ-GFP or TFAM-GFP and imaged 36h later. Still images show diffuse staining
657 of TFAM-GFP upon ddC treatment, indicating relocalization. mt- α FtsZ-GFP forms puncta
658 irrespective of ddC treatment. Inset enlarged 2x. Scalebar: 10 μ m.

659 **D**

660 Time lapse imaging of the same cells depicted in C, showing 4x enlarged insets with mt-
661 α FtsZ-GFP localization at fission sites in both control and ddC treated cells.

662

663 **Fig 4: Identification of mt- α FtsZ interaction partners that play a role in**
664 **mitochondrial fission**

665 **A**

666 Number of proteins obtained by mass-spectrometry analysis of mt- α FtsZ-Flag versus
667 mtGFP-Flag immunoprecipitates. Grey indicates proteins identified in mt- α FtsZ-Flag and
668 absent in mtGFP-Flag immunoprecipitates, black indicates proteins that are significantly
669 enriched in mt- α FtsZ-Flag versus mtGFP-Flag immunoprecipitates.

670 **B**

671 GO-term analysis of proteins identified through mt- α FtsZ-Flag immunoprecipitation
672 (Panther software).

673 **C**

674 Semiautomated quantification (MiNA plugin) of mitochondrial morphology expressed
675 by the amount of individual mitochondria/mitochondrial area in U2OS cells transfected
676 with mtGFP or inner membrane proteins PGAM5, FAM210A, MTCH1, SFXN3 and DAPIT.
677 Three experiments were pooled. Mean and SEM are displayed in red. $P < 0.0001$ by one-
678 way Anova, adjusted P-values < 0.0001 .

679 **D**

680 U2OS cells expressing very low amounts of fission-inducing constructs PGAM5,
681 FAM210A, MTCH1, SFXN3, shown in green. Mitochondria are shown in red (Hsp60) .

682 Scalebar: 10 μ m, insets enlarged 4x. Linescans (yellow) show varying levels of
683 accumulation at constrictions.

684

685 **Supplementary Figure legends**

686

687 **Suppl Fig1: Characterization of mt- α FtsZ localization and their impact on** 688 **mitochondrial morphology**

689 **A**

690 Cytosolic mt- α FtsZ-Flag (green) colocalizes with tubulin (red). Scalebar: 10 μ m, insets
691 enlarged 3x.

692 **B**

693 Perinuclear aggregation of mitochondria in cells where mt- α FtsZ-GFP mislocalizes to the
694 cytosol. Immunofluorescence of U2OS cells transiently expressing mt- α FtsZ-GFP (green)
695 and labeled for Hsp60 (mitochondria, red). The percentage of cells displaying cytosolic
696 filaments increased to 20.2 \pm 10.5% (n=1361, N=4) when GFP was employed instead of
697 the flag tag. Scalebar: 10 μ m, insets enlarged 3x.

698 **C**

699 Representative example of a cell displaying diffuse mt- α FtsZ Δ CT-Flag (green) staining in
700 mitochondria. Mitochondria are shown in red (Hsp60). Scalebar: 10 μ m, insets enlarged
701 3x.

702 **D**

703 Mitochondrial constrictions in Hela cells expressing intermediate levels of mt- α FtsZ-GFP
704 or mt-GFP analyzed by HPF-CLEM. Inner diameters (ID) and outer diameters (OD) are
705 indicated in yellow. Scalebar: 100nm.

706 **E**

707 MiNA analysis of mitochondrial branch length in U2OS cells transfected with mito-GFP-
708 Flag or mitochondrially targeted FtsZ from a gamma- (mt- γ FtsZ-Flag) or
709 alphaproteobacterium (mt- α FtsZ-Flag, C-terminal deletion mutant mt- α FtsZ Δ CT-Flag).
710 The same dataset was used as in Fig 1C. Mean and SEM are displayed in red, p<0.0001
711 by one-way Anova, adjusted P-value <0.0001.

712

713

714

715 **F**

716 Manual measurement of the length of resolvable mitochondria in HeLa cells expressing
717 mt- α FtsZ-Flag and counterstained for mitochondria (Hsp60). n>60, N=5. Mean and SEM
718 are shown in red, P<0.0001 by one-way Anova, adjusted P-values <0.0001.

719

720 **Suppl Fig 2: Differential effect of mt- α FtsZ on the outer membrane and the**
721 **mitochondrial matrix**

722 HeLa cells labeled for mt- α FtsZ-Flag (green) display matrix constriction (Hsp60, red) in
723 the absence of outer membrane (Tom20, blue) constriction

724

725 **Suppl Fig 3: mt- α FtsZ-labeled constrictions are flanked by mtDNA**

726 U2OS cells transfected with mt- α FtsZ-GFP (green) and labeled for mtDNA (red) and
727 mitotracker deep red (blue). Insets enlarged 2x. Linescans showing mt- α FtsZ-GFP
728 localization at mitochondrial constrictions, flanked by mtDNA.

729

730 **Suppl Fig 4: Functional annotation of mt- α FtsZ interaction partners and**
731 **overexpression of selected proteins**

732 **A**

733 Functional annotation clusters ("Biological Process", BP) of proteins co-
734 immunoprecipitating with mt- α FtsZ-Flag assessed in the background of the human
735 proteome (DAVID software).

736 The 4 most enriched clusters are shown, with associated keywords and GO terms. Black
737 bars show % protein count and grey bars show fold enrichment. Benjamini scores are
738 shown on the far right. All p-values were<0.01.

739 **B**

740 Representative images of U2OS cells transfected with flag-tagged versions of the inner
741 membrane proteins FAM210A, MTCH1, PGAM5, SFXN3 and DAPIT (shown in green) and
742 quantified in Fig 4D. Mitochondria were labeled with Hsp60 (red) and appear
743 fragmented by FAM210A, MTCH1, PGAM5 or SFXN3 expression.

744

745

746

747

748 **References**

- 749 1. Sagan, L. On the origin of mitosing cells. *J. Theor. Biol.* 14, 255–274 (1967).
750 2. Muñoz-Gómez, S. A., Wideman, J. G., Roger, A. J. & Slamovits, C. H. The Origin of
751 Mitochondrial Cristae from Alphaproteobacteria. *Mol. Biol. Evol.* 34, 943–956 (2017).
752 3. Bi, E. F. & Lutkenhaus, J. FtsZ ring structure associated with division in Escherichia
753 coli. *Nature* 354, 161–164 (1991).
754 4. Löwe, J. & Amos, L. A. Crystal structure of the bacterial cell-division protein FtsZ.
755 *Nature* 391, 203–206 (1998).
756 5. Mukherjee, A. & Lutkenhaus, J. Purification, assembly, and localization of FtsZ. *Meth.*
757 *Enzymol.* 298, 296–305 (1998).
758 6. Egan, A. J. F. & Vollmer, W. The physiology of bacterial cell division. *Ann. N. Y. Acad.*
759 *Sci.* 1277, 8–28 (2013).
760 7. Du, S. & Lutkenhaus, J. At the Heart of Bacterial Cytokinesis: The Z Ring. *Trends*
761 *Microbiol.* 27, 781–791 (2019).
762 8. Pagliuso, A., Cossart, P. & Stavru, F. The ever-growing complexity of the
763 mitochondrial fission machinery. *Cell Mol Life Sci* 75, 355–374 (2018).
764 9. Wai, T. & Langer, T. Mitochondrial Dynamics and Metabolic Regulation. *Trends in*
765 *endocrinology and metabolism: TEM* 27, 105–117 (2016).
766 10. Leger, M. M. *et al.* An ancestral bacterial division system is widespread in eukaryotic
767 mitochondria. *Proc. Natl. Acad. Sci. U.S.A.* 112, 10239–10246 (2015).
768 11. Pernas, L. & Scorrano, L. Mito-Morphosis: Mitochondrial Fusion, Fission, and Cristae
769 Remodeling as Key Mediators of Cellular Function. *Annu. Rev. Physiol.* 78, 505–531
770 (2016).
771 12. Nishida, K. *et al.* Triple immunofluorescent labeling of FtsZ, dynamin, and EF-Tu
772 reveals a loose association between the inner and outer membrane mitochondrial
773 division machinery in the red alga Cyanidioschyzon merolae. *J. Histochem. Cytochem.*
774 52, 843–849 (2004).
775 13. Nishida, K. *et al.* Dynamic recruitment of dynamin for final mitochondrial severance
776 in a primitive red alga. *Proc. Natl. Acad. Sci. U.S.A.* 100, 2146–2151 (2003).
777 14. Lee, J. E., Westrate, L. M., Wu, H., Page, C. & Voeltz, G. K. Multiple dynamin family
778 members collaborate to drive mitochondrial division. *Nature* 540, 139–143 (2016).
779 15. Kamerkar, S. C., Kraus, F., Sharpe, A. J., Pucadyil, T. J. & Ryan, M. T. Dynamin-related
780 protein 1 has membrane constricting and severing abilities sufficient for
781 mitochondrial and peroxisomal fission. *Nat Commun* 9, 5239 (2018).
782 16. Fonseca, T. B., Sánchez-Guerrero, Á., Milosevic, I. & Raimundo, N. Mitochondrial
783 fission requires DRP1 but not dynamins. *Nature* 570, E34–E42 (2019).
784 17. Mahecic, D. *et al.* Membrane bending energy and tension govern mitochondrial
785 division. *bioRxiv* 255356 (2019) doi:10.1101/255356.
786 18. Takahara, M. *et al.* A putative mitochondrial ftsZ gene is present in the unicellular
787 primitive red alga Cyanidioschyzon merolae. *Mol. Gen. Genet.* 264, 452–460 (2000).
788 19. Beech, P. L. *et al.* Mitochondrial FtsZ in a chromophyte alga. *Science* 287, 1276–1279
789 (2000).
790 20. Gilson, P. R. *et al.* Two Dictyostelium orthologs of the prokaryotic cell division
791 protein FtsZ localize to mitochondria and are required for the maintenance of
792 normal mitochondrial morphology. *Eukaryotic Cell* 2, 1315–1326 (2003).
793 21. Kiefel, B. R., Gilson, P. R. & Beech, P. L. Diverse eukaryotes have retained
794 mitochondrial homologues of the bacterial division protein FtsZ. *Protist* 155, 105–
795 115 (2004).

- 796 22. Chan, D. C. Fusion and fission: interlinked processes critical for mitochondrial health.
797 *Annu. Rev. Genet.* 46, 265–287 (2012).
- 798 23. Legesse-Miller, A., Massol, R. H. & Kirchhausen, T. Constriction and Dnm1p
799 recruitment are distinct processes in mitochondrial fission. *Mol. Biol. Cell* 14, 1953–
800 1963 (2003).
- 801 24. Labrousse, A. M., Zappaterra, M. D., Rube, D. A. & van der Bliek, A. M. C. elegans
802 dynamin-related protein DRP-1 controls severing of the mitochondrial outer
803 membrane. *Mol. Cell* 4, 815–826 (1999).
- 804 25. Malka, F. *et al.* Separate fusion of outer and inner mitochondrial membranes. *EMBO*
805 *Rep.* 6, 853–859 (2005).
- 806 26. Cho, B. *et al.* Constriction of the mitochondrial inner compartment is a priming event
807 for mitochondrial division. *Nat Commun* 8, 15754 (2017).
- 808 27. Purkanti, R. & Thattai, M. Ancient dynamin segments capture early stages of host-
809 mitochondrial integration. *Proc. Natl. Acad. Sci. U.S.A.* 112, 2800–2805 (2015).
- 810 28. Andersson, S. G. *et al.* The genome sequence of *Rickettsia prowazekii* and the origin
811 of mitochondria. *Nature* 396, 133–140 (1998).
- 812 29. Sasser, D. *et al.* Phylogenomic evidence for the presence of a flagellum and cbb(3)
813 oxidase in the free-living mitochondrial ancestor. *Mol. Biol. Evol.* 28, 3285–3296
814 (2011).
- 815 30. Wang, Z. & Wu, M. An integrated phylogenomic approach toward pinpointing the
816 origin of mitochondria. *Sci Rep* 5, 1–12 (2015).
- 817 31. Williams, K. P., Sobral, B. W. & Dickerman, A. W. A robust species tree for the
818 alphaproteobacteria. *J. Bacteriol.* 189, 4578–4586 (2007).
- 819 32. Fitzpatrick, D. A., Creevey, C. J. & McInerney, J. O. Genome phylogenies indicate a
820 meaningful alpha-proteobacterial phylogeny and support a grouping of the
821 mitochondria with the Rickettsiales. *Mol. Biol. Evol.* 23, 74–85 (2006).
- 822 33. Ferla, M. P., Thrash, J. C., Giovannoni, S. J. & Patrick, W. M. New rRNA gene-based
823 phylogenies of the Alphaproteobacteria provide perspective on major groups,
824 mitochondrial ancestry and phylogenetic instability. *PLoS ONE* 8, e83383 (2013).
- 825 34. Martijn, J., Vosseberg, J., Guy, L., Offre, P. & Ettema, T. J. G. Deep mitochondrial origin
826 outside the sampled alphaproteobacteria. *Nature* 557, 101–105 (2018).
- 827 35. Ma, X. & Margolin, W. Genetic and Functional Analyses of the Conserved C-Terminal
828 Core Domain of *Escherichia coli* FtsZ. *Journal of Bacteriology* 181, 7531 (1999).
- 829 36. Spelbrink, J. N. *et al.* Human mitochondrial DNA deletions associated with mutations
830 in the gene encoding Twinkle, a phage T7 gene 4-like protein localized in
831 mitochondria. *Nat. Genet.* 28, 223–231 (2001).
- 832 37. Margineantu, D. H. *et al.* Cell cycle dependent morphology changes and associated
833 mitochondrial DNA redistribution in mitochondria of human cell lines.
834 *Mitochondrion* 1, 425–435 (2002).
- 835 38. Rajala, N., Gerhold, J. M., Martinsson, P., Klymov, A. & Spelbrink, J. N. Replication
836 factors transiently associate with mtDNA at the mitochondrial inner membrane to
837 facilitate replication. *Nucleic Acids Res* 42, 952–967 (2014).
- 838 39. Lewis, S. C., Uchiyama, L. F. & Nunnari, J. ER-mitochondria contacts couple mtDNA
839 synthesis with mitochondrial division in human cells. *Science* 353, aaf5549 (2016).
- 840 40. Murley, A. *et al.* ER-associated mitochondrial division links the distribution of
841 mitochondria and mitochondrial DNA in yeast. *Elife* 2, e00422 (2013).
- 842 41. Ban-Ishihara, R., Ishihara, T., Sasaki, N., Mihara, K. & Ishihara, N. Dynamics of
843 nucleoid structure regulated by mitochondrial fission contributes to cristae

- 844 reformation and release of cytochrome c. *Proc. Natl. Acad. Sci. U.S.A.* 110, 11863–
845 11868 (2013).
- 846 42. Yu, X. C., Margolin, W., Gonzalez-Garay, M. L. & Cabral, F. Vinblastine induces an
847 interaction between FtsZ and tubulin in mammalian cells. *J. Cell. Sci.* 112 (Pt 14),
848 2301–2311 (1999).
- 849 43. Calvo, S. E., Clauser, K. R. & Mootha, V. K. MitoCarta2.0: an updated inventory of
850 mammalian mitochondrial proteins. *Nucleic Acids Res.* 44, D1251-1257 (2016).
- 851 44. Smith, A. C. & Robinson, A. J. MitoMiner v3.1, an update on the mitochondrial
852 proteomics database. *Nucleic Acids Res.* 44, D1258-1261 (2016).
- 853 45. Itoh, K., Tamura, Y., Iijima, M. & Sesaki, H. Effects of Fcj1-Mos1 and mitochondrial
854 division on aggregation of mitochondrial DNA nucleoids and organelle morphology.
855 *Mol. Biol. Cell* 24, 1842–1851 (2013).
- 856 46. Li, H. *et al.* Mic60/Mitofilin determines MICOS assembly essential for mitochondrial
857 dynamics and mtDNA nucleoid organization. *Cell Death Differ.* 23, 380–392 (2016).
- 858 47. Wai, T. *et al.* The membrane scaffold SLP2 anchors a proteolytic hub in mitochondria
859 containing PARL and the i-AAA protease YME1L. *EMBO Rep.* 17, 1844–1856 (2016).
- 860 48. James, D. I., Parone, P. A., Mattenberger, Y. & Martinou, J.-C. hFis1, a novel component
861 of the mammalian mitochondrial fission machinery. *J. Biol. Chem.* 278, 36373–36379
862 (2003).
- 863 49. Tondera, D. *et al.* The mitochondrial protein MTP18 contributes to mitochondrial
864 fission in mammalian cells. *J. Cell. Sci.* 118, 3049–3059 (2005).
- 865 50. Harel, T. *et al.* Recurrent De Novo and Biallelic Variation of ATAD3A, Encoding a
866 Mitochondrial Membrane Protein, Results in Distinct Neurological Syndromes. *Am. J.*
867 *Hum. Genet.* 99, 831–845 (2016).
- 868 51. Banfi, S. *et al.* Identification and characterization of AFG3L2, a novel paraplegin-
869 related gene. *Genomics* 59, 51–58 (1999).
- 870 52. Osawa, M. & Erickson, H. P. Liposome division by a simple bacterial division
871 machinery. *Proc. Natl. Acad. Sci. U.S.A.* 110, 11000–11004 (2013).
- 872 53. Sugo, M. *et al.* Syntaxin 17 regulates the localization and function of PGAM5 in
873 mitochondrial division and mitophagy. *EMBO J.* 37, (2018).
- 874 54. Ruiz, K. *et al.* Functional role of PGAM5 multimeric assemblies and their
875 polymerization into filaments. *Nat Commun* 10, 531 (2019).
- 876 55. Wilkins, J. M., McConnell, C., Tipton, P. A. & Hannink, M. A conserved motif mediates
877 both multimer formation and allosteric activation of phosphoglycerate mutase 5. *J.*
878 *Biol. Chem.* 289, 25137–25148 (2014).
- 879 56. Kory, N. *et al.* SFXN1 is a mitochondrial serine transporter required for one-carbon
880 metabolism. *Science* 362, (2018).
- 881 57. Erickson, H. P., Anderson, D. E. & Osawa, M. FtsZ in bacterial cytokinesis:
882 cytoskeleton and force generator all in one. *Microbiol. Mol. Biol. Rev.* 74, 504–528
883 (2010).
- 884 58. Trueba, F. J. & Woldringh, C. L. Changes in cell diameter during the division cycle of
885 *Escherichia coli*. *J Bacteriol* 142, 869–878 (1980).
- 886 59. Jans, D. C. *et al.* STED super-resolution microscopy reveals an array of MINOS
887 clusters along human mitochondria. *Proc. Natl. Acad. Sci. U.S.A.* 110, 8936–8941
888 (2013).
- 889 60. *Manual of Clinical Microbiology, Eleventh Edition.* (American Society of Microbiology,
890 2015). doi:10.1128/9781555817381.
- 891 61. Eswara, P. J. & Ramamurthi, K. S. Bacterial Cell Division: Nonmodels Poised to Take
892 the Spotlight. *Annu. Rev. Microbiol.* 71, 393–411 (2017).

- 893 62. Kuroiwa, T. Mechanisms of organelle division and inheritance and their implications
894 regarding the origin of eukaryotic cells. *Proc. Jpn. Acad., Ser. B, Phys. Biol. Sci.* 86,
895 455–471 (2010).
- 896 63. Pazos, M. *et al.* FtsZ placement in nucleoid-free bacteria. *PLoS ONE* 9, e91984 (2014).
- 897 64. Lu, C., Reedy, M. & Erickson, H. P. Straight and curved conformations of FtsZ are
898 regulated by GTP hydrolysis. *J. Bacteriol.* 182, 164–170 (2000).
- 899 65. Osawa, M., Anderson, D. E. & Erickson, H. P. Reconstitution of contractile FtsZ rings
900 in liposomes. *Science* 320, 792–794 (2008).
- 901 66. Coltharp, C., Buss, J., Plumer, T. M. & Xiao, J. Defining the rate-limiting processes of
902 bacterial cytokinesis. *Proc. Natl. Acad. Sci. U.S.A.* 113, E1044–1053 (2016).
- 903 67. Bisson-Filho, A. W. *et al.* Treadmilling by FtsZ filaments drives peptidoglycan
904 synthesis and bacterial cell division. *Science* 355, 739–743 (2017).
- 905 68. Yang, X. *et al.* GTPase activity-coupled treadmilling of the bacterial tubulin FtsZ
906 organizes septal cell wall synthesis. *Science* 355, 744–747 (2017).
- 907 69. Becker, T., Gebert, M., Pfanner, N. & van der Laan, M. Biogenesis of mitochondrial
908 membrane proteins. *Curr. Opin. Cell Biol.* 21, 484–493 (2009).
- 909 70. Gilquin, B. *et al.* The calcium-dependent interaction between S100B and the
910 mitochondrial AAA ATPase ATAD3A and the role of this complex in the cytoplasmic
911 processing of ATAD3A. *Mol. Cell. Biol.* 30, 2724–2736 (2010).
- 912 71. Wang, Y. & Bogenhagen, D. F. Human mitochondrial DNA nucleoids are linked to
913 protein folding machinery and metabolic enzymes at the mitochondrial inner
914 membrane. *J. Biol. Chem.* 281, 25791–25802 (2006).
- 915 72. Ji, W., Hatch, A. L., Merrill, R. A., Strack, S. & Higgs, H. N. Actin filaments target the
916 oligomeric maturation of the dynamin GTPase Drp1 to mitochondrial fission sites.
917 *Elife* 4, e11553 (2015).
- 918 73. Yu, X. C. & Margolin, W. Ca²⁺-mediated GTP-dependent dynamic assembly of
919 bacterial cell division protein FtsZ into asters and polymer networks in vitro. *EMBO*
920 *J.* 16, 5455–5463 (1997).
- 921 74. Valente, A. J., Maddalena, L. A., Robb, E. L., Moradi, F. & Stuart, J. A. A simple ImageJ
922 macro tool for analyzing mitochondrial network morphology in mammalian cell
923 culture. *Acta Histochemica* 119, 315–326 (2017).
- 924 75. McDonald, K. *et al.* ‘Tips and tricks’ for high-pressure freezing of model systems.
925 *Methods Cell Biol.* 96, 671–693 (2010).
- 926 76. Pagliuso, A. *et al.* A role for septin 2 in Drp1-mediated mitochondrial fission. *EMBO*
927 *Rep* 17, 858–73 (2016).
- 928 77. Lago, M. *et al.* Proteome remodelling by the stress sigma factor RpoS/σS in
929 *Salmonella*: identification of small proteins and evidence for post-transcriptional
930 regulation. *Sci Rep* 7, 2127 (2017).
- 931 78. Tyanova, S., Temu, T. & Cox, J. The MaxQuant computational platform for mass
932 spectrometry-based shotgun proteomics. *Nat Protoc* 11, 2301–2319 (2016).
- 933 79. Vizcaino, J. A. *et al.* 2016 update of the PRIDE database and its related tools. *Nucleic*
934 *Acids Res.* 44, 11033 (2016).
- 935 80. Wieczorek, S. *et al.* DAPAR & ProStaR: software to perform statistical analyses in
936 quantitative discovery proteomics. *Bioinformatics* 33, 135–136 (2017).
- 937 81. Ritchie, M. E. *et al.* limma powers differential expression analyses for RNA-
938 sequencing and microarray studies. *Nucleic Acids Res.* 43, e47 (2015).
- 939 82. Giai Gianetto, Q. *et al.* Calibration plot for proteomics: A graphical tool to visually
940 check the assumptions underlying FDR control in quantitative experiments.
941 *Proteomics* 16, 29–32 (2016).

942 83. Friedman, J. R. *et al.* ER tubules mark sites of mitochondrial division. *Science* 334,
943 358–362 (2011).
944

Figure 1

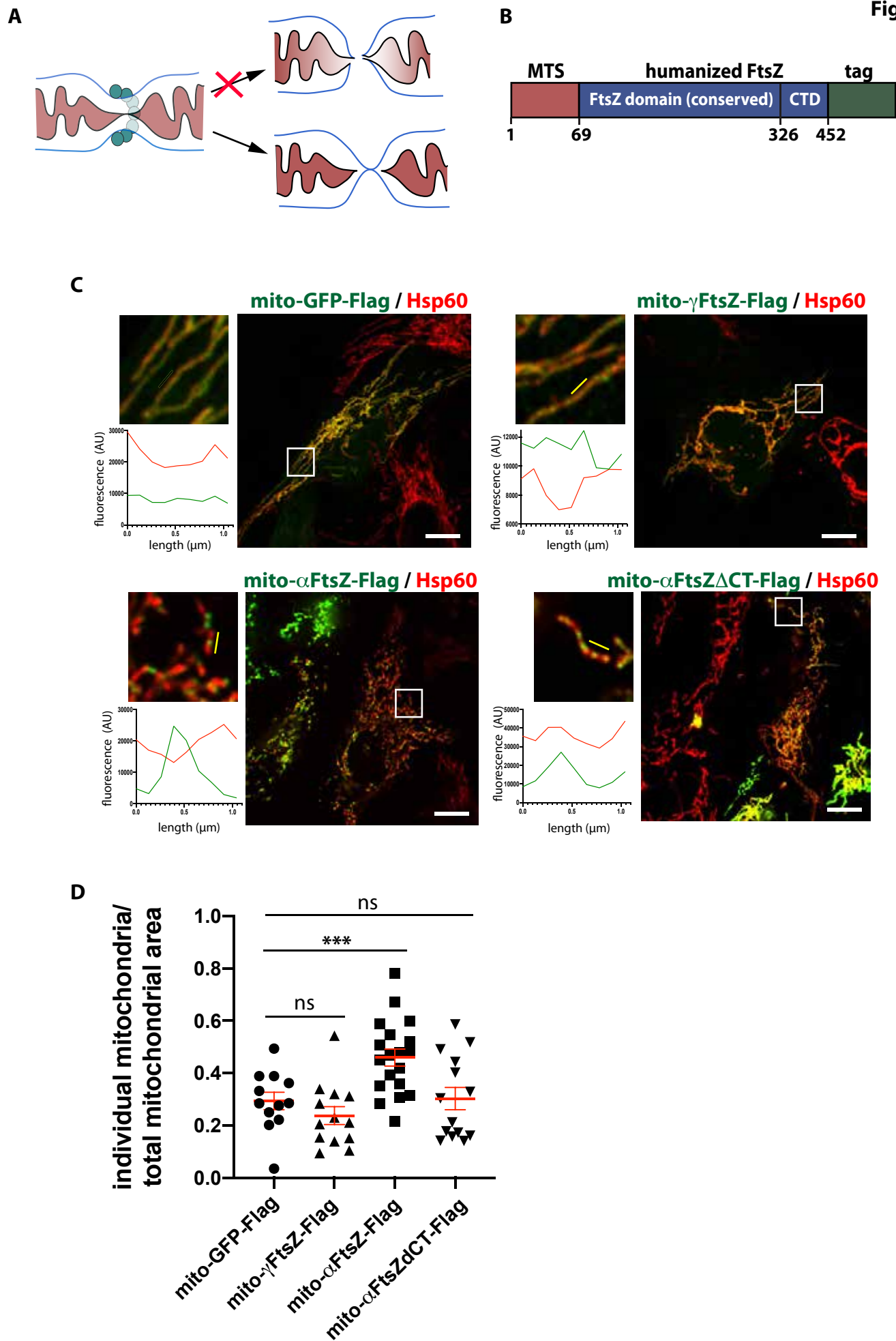


Figure 2

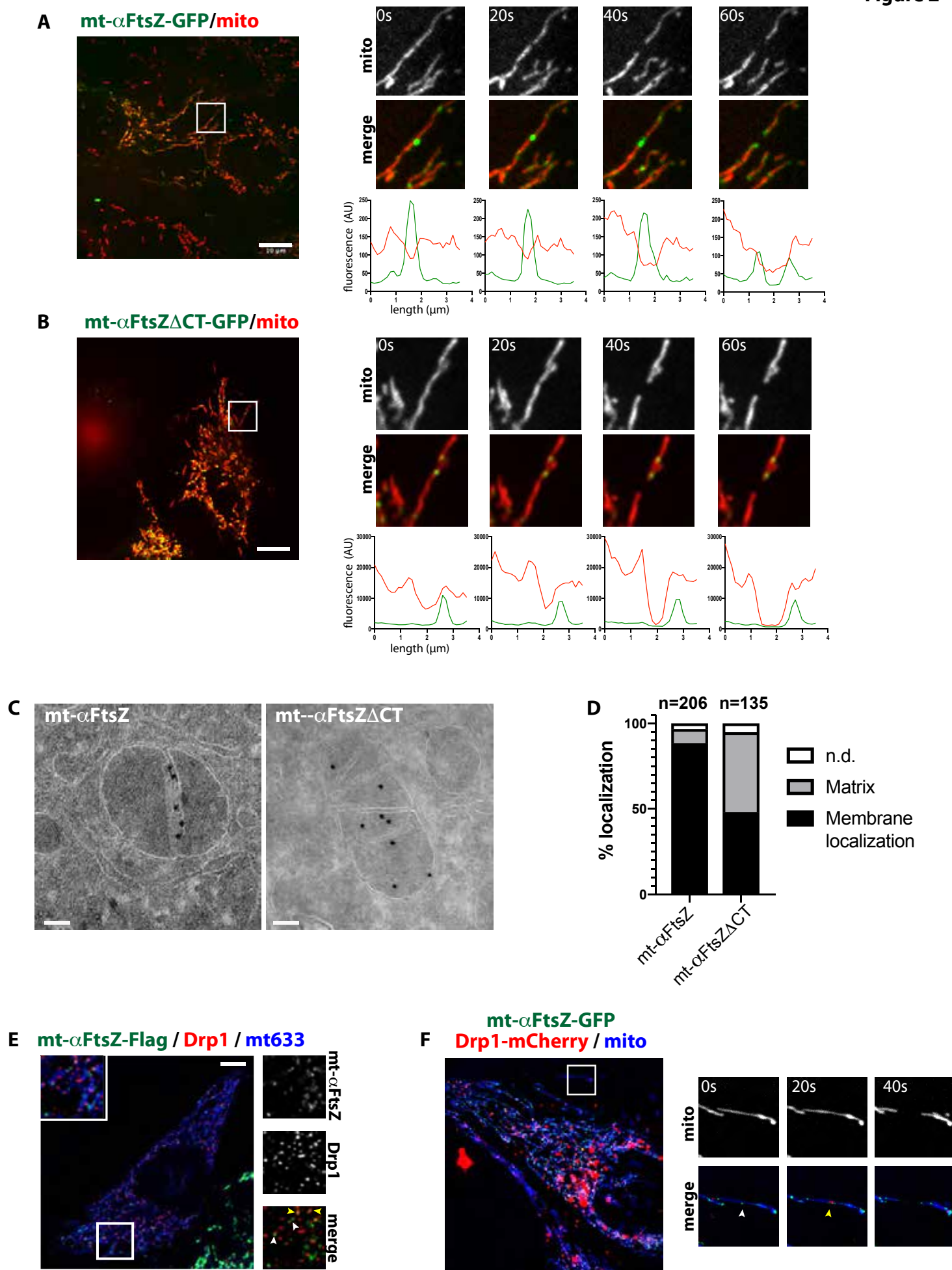


Figure 3

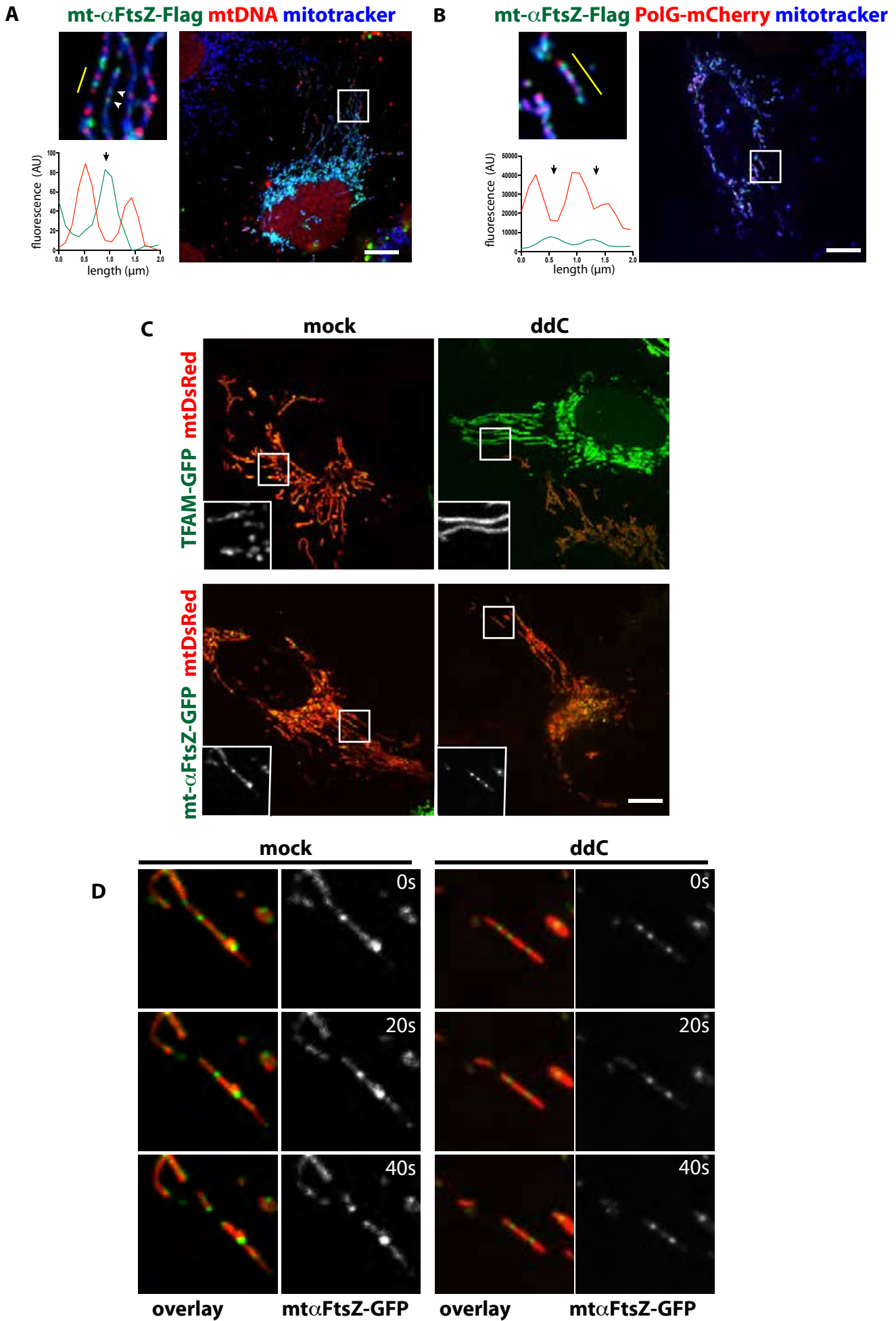
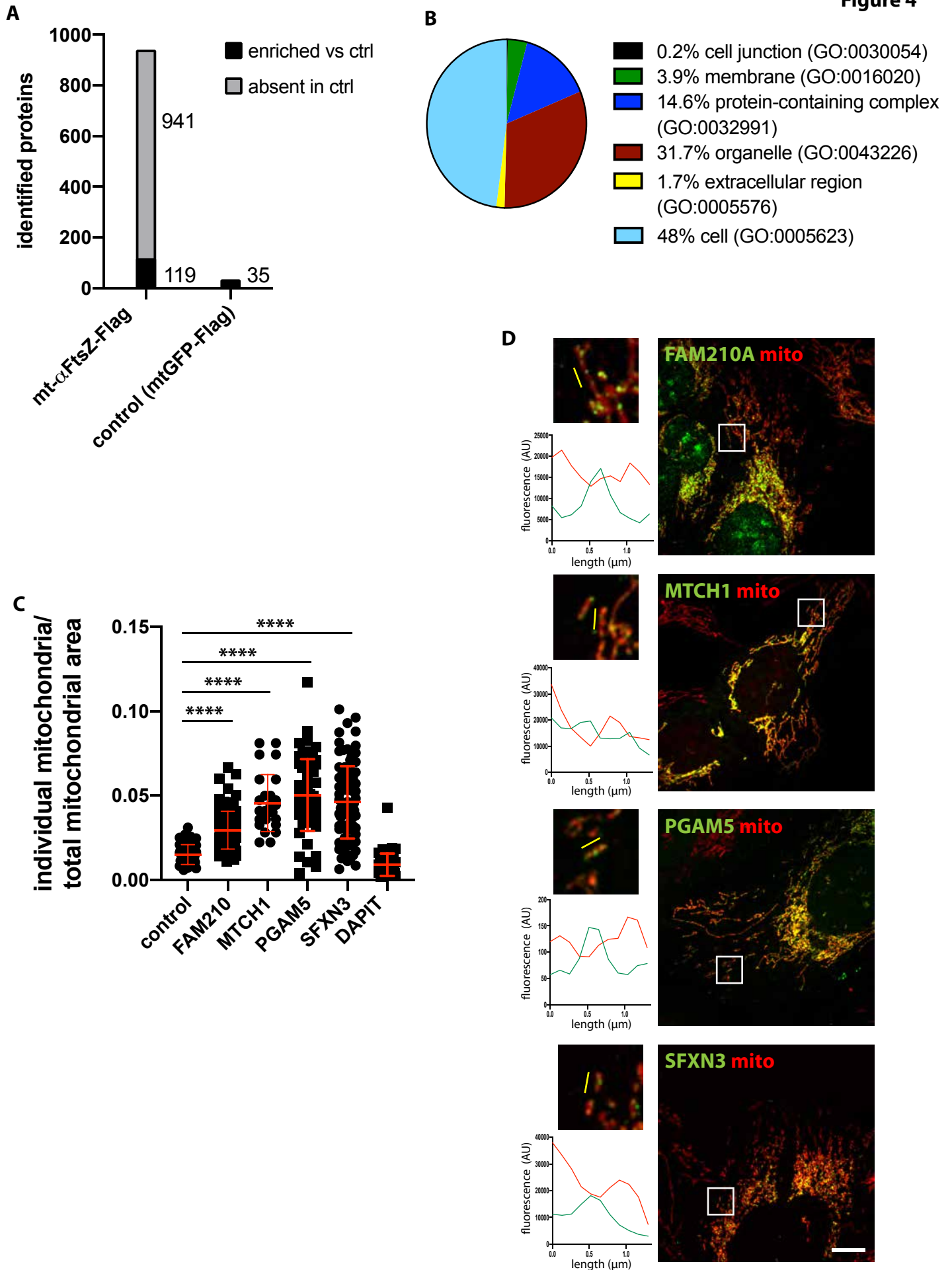
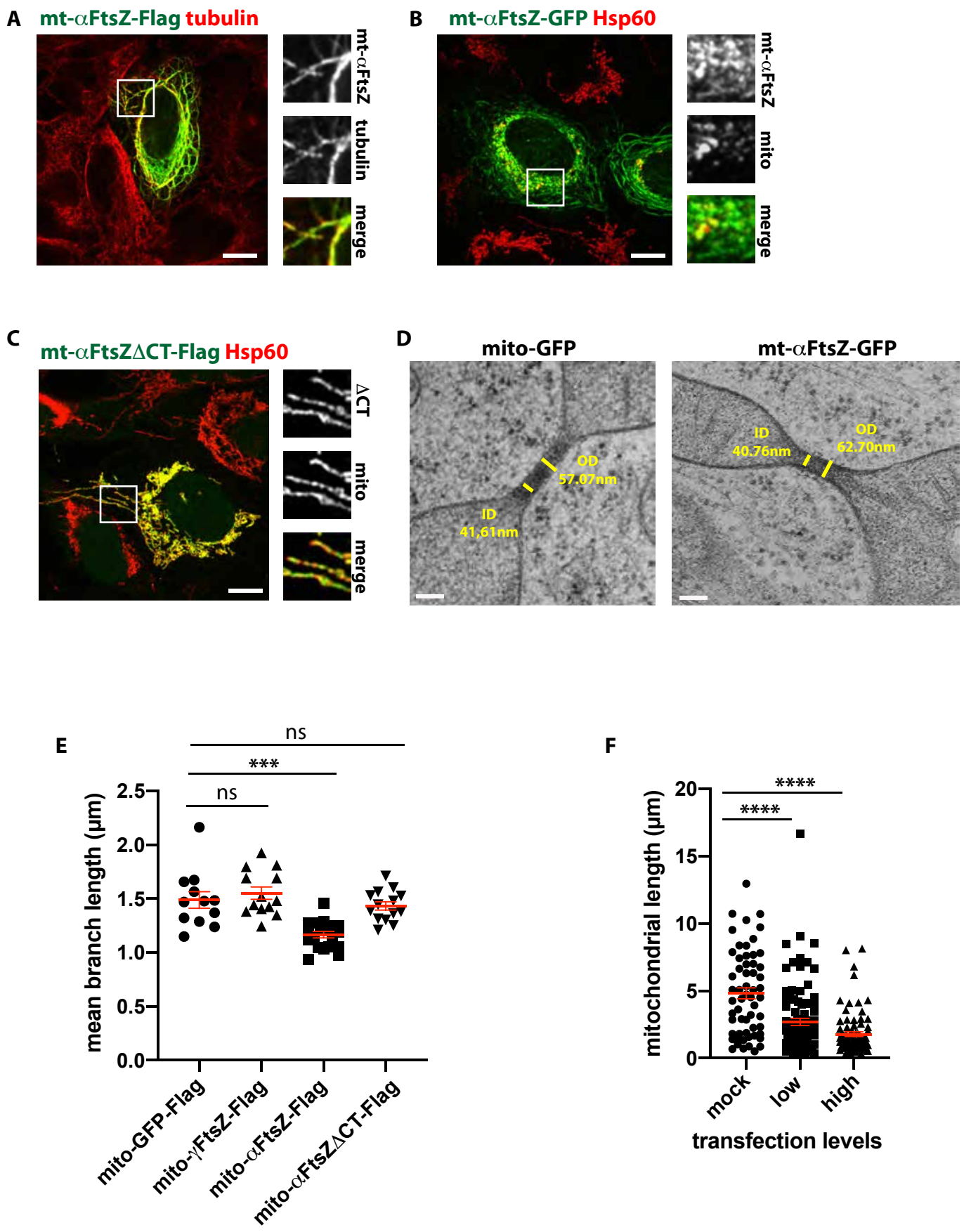


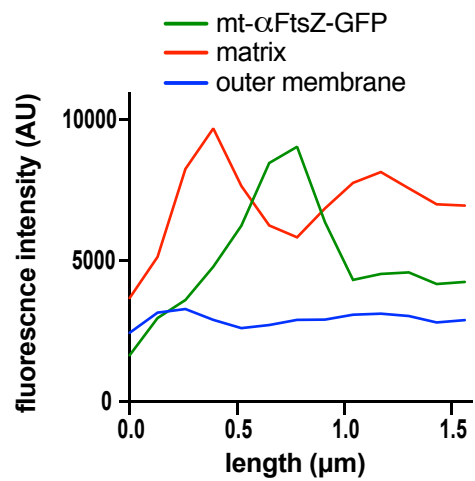
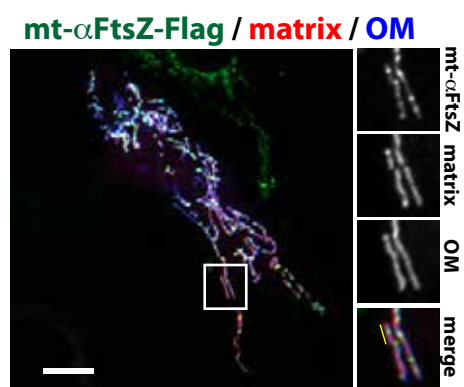
Figure 4



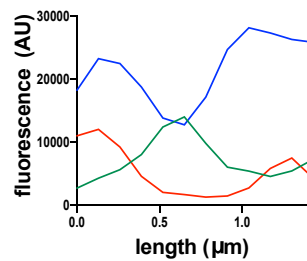
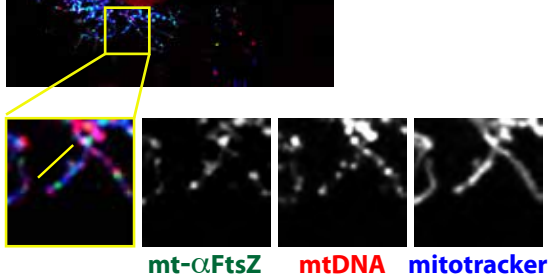
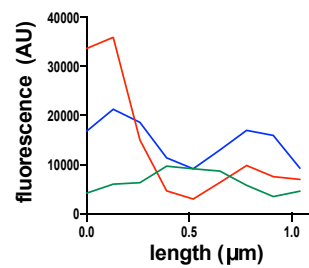
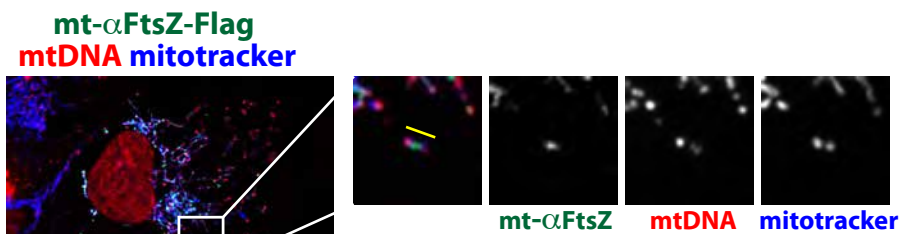
Suppl. Fig 1



Supplementary Fig 2

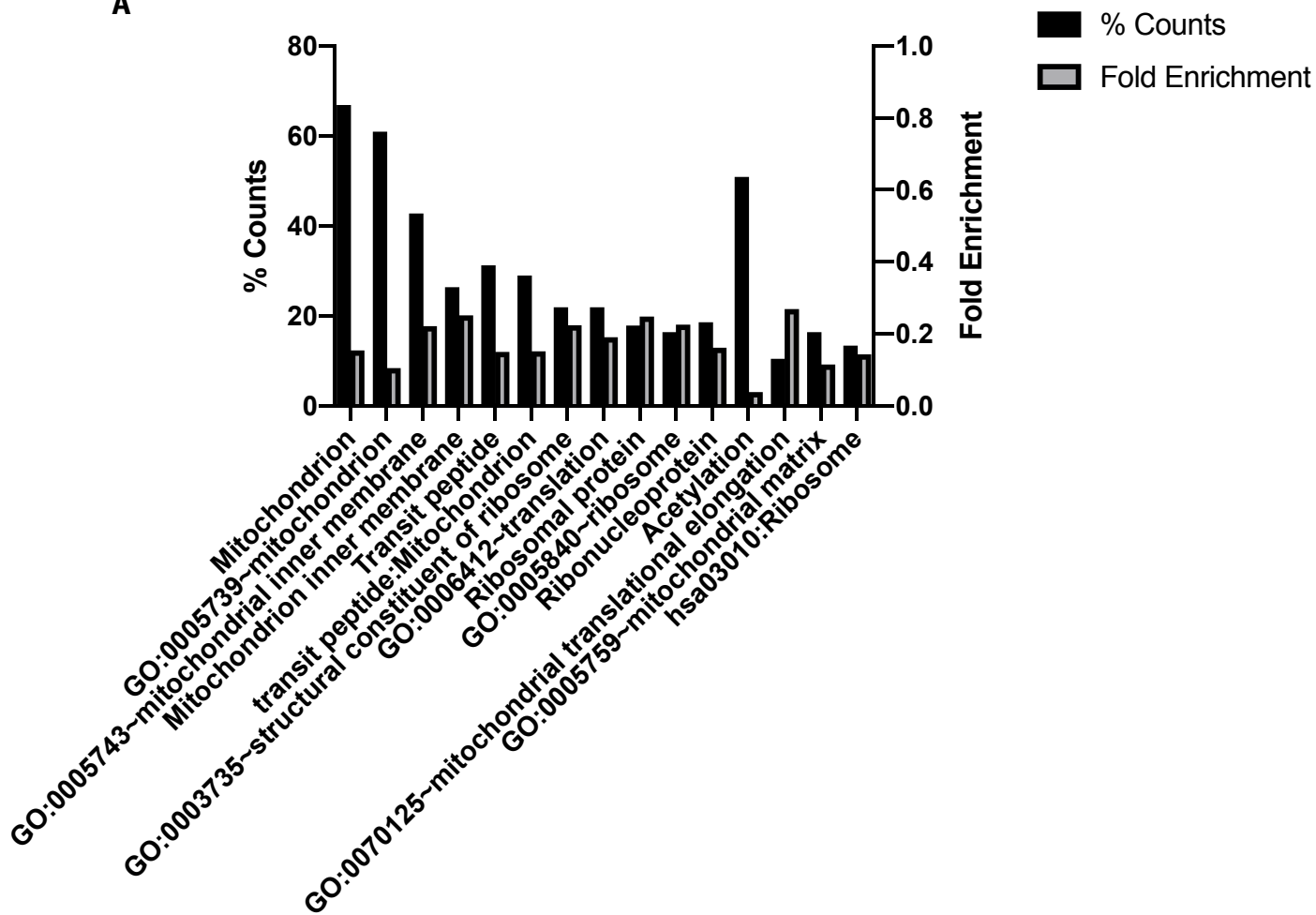


Suppl Fig 3



Supplementary Figure 4

A



B

